Received: 3 April 2019 | Revised: 29 July 2019 | Accepted: 2 August 2019

DOI: 10.1111/cas.14162

ORIGINAL ARTICLE

Cancer Science WILEY

In vivo selection reveals autophagy promotes adaptation of metastatic ovarian cancer cells to abdominal microenvironment

Chih-Lin Kuo | Zhe-Yu Jiang | Ying-Wen Wang | Ting-Yu Lin | Wei-Lin Huang | Fang-Ju Wu | Ching-Wei Luo

Department of Life Sciences and Institute of Genome Sciences, National Yang-Ming University, Taipei, Taiwan

Correspondence
Ching-Wei Luo, Department of Life Sciences and Institute of Genome Sciences, National Yang-Ming University, 155 Li-Nong Street, Section 2, Beitou, Taipei 112, Taiwan.
Email: cwluo@ym.edu.tw

Funding information
Ministry of Science and Technology in Taiwan, Grant/Award Number: MOST 107-2314-B-010-016-MY3 and MOST 107-2627-M-400-001; Ministry of Education, Aim for the Top University Plan in Taiwan., Grant/Award Number: 106AC-D106

Abstract

Peritoneal dissemination is the most frequent metastatic route of ovarian cancer. However, due to the high heterogeneity in ovarian cancer, most conventional studies lack parental tumor controls relevant to metastases and, thus, it is difficult to trace the molecular changes of cancer cells along with the selection by the abdominal microenvironment. Here, we established an in vivo mouse peritoneal dissemination scheme that allowed us to select more aggressive sublines from parental ovarian cancer cells, including A2780 and SKOV-3. Microarray and gene profiling analyses indicated that autophagy-related genes were enriched in selected malignant sublines. Detection of LC3-II, p62 and autophagic puncta demonstrated that these malignant variants were more sensitive to autophagic induction when exposed to diverse stress conditions, such as high cell density, starvation and drug treatment. As compared with parental A2780, the selected variant acquired the ability to grow better under high-density stress; however, this effect was reversed by addition of autophagic inhibitors or knockdown of *ATG5*. When analyzing the clinical profiles of autophagy-related genes identified to be enriched in malignant A2780 variant, 73% of them had prognostic significance for the survival of ovarian cancer patients. Taken together, our findings indicate that an increase in autophagic potency among ovarian cancer cells is crucial for selection of metastatic colonies in the abdominal microenvironment. In addition, the derived autophagic gene profile can not only predict prognosis well but can also be potentially applied to precision medicine for identifying those ovarian cancer patients suitable for taking anti–autophagy cancer drugs.

KEYWORDS
autophagy, in vivo selection, LC3-II, metastasis, ovarian cancer

1 | INTRODUCTION

Ovarian cancer accounts for 2% of cancers that affect women worldwide.[1] More than 90% of ovarian cancer is of epithelial origin.[2] According to the latest cancer statistics from the United States, ovarian cancer is the 11th most common cancer among women in the United States; however, its mortality ranks 5th among cancer-related deaths and has always been the highest among gynecological

Jiang and Wang contributed equally to this work.

cancers.[3] The poor outcomes among these patients are partly due to the frequent occurrence of dissemination before there is a diagnosis. Indeed, clinical reports indicate that more than 60% of all cases of ovarian cancer are diagnosed at an advanced stage, which is characterized by extensive invasion and metastasis. The metastases normally proliferate rapidly and show a high incidence of chemoresistance[4]; this, in turn, leads to a 5-year survival rate for these patients of less than 29%.[3]

The precise molecular mechanisms that promote ovarian cancer dissemination remain undefined. Nevertheless, it is becoming clear that ovarian cancer can disseminate passively by movement of peritoneal fluid in the abdominal cavity.[5] Therefore, the task of ovarian cancer metastasis appears to be easier than that of the classic pattern of hematogenous metastasis, which has been well studied for most other solid cancers.[6] In addition, ovarian cancer is often accompanied by malignant ascites, which can be found in more than one-third of patients at the time of diagnosis and in almost all patients at recurrence.[7,8] The forming ascites further provides a complicated liquid environment that not only accelerates transportation of cancer cells to distant sites but also supports their survival before implantation.[9-11] Although it is easy to spread intra-abdominally, the detached ovarian cancer cells still need to overcome multiple challenges, such as evading anoikis, invading the mesothelium for implantation, inducing angiogenesis and undergoing proliferative outgrowth, in order to form metastatic tumors.[5,9] Any increase in the ability to carry out any of the above steps will greatly promote the malignancy of a given ovarian cancer.

It has been widely accepted that tumor masses contain heterogeneous subpopulations of cancer cells and these subpopulations have different potentials in terms of malignancy.[12-14] Thus, it can be postulated that the outcome of ovarian cancer metastasis may result from the survival and expansion of specialized colonies with particular properties that preexist in the parental tumor and have then undergone multiple selective steps. However, how these specialized colonies evolve to adapt to the abdominal microenvironment and to interact with the tissue at the metastatic sites remain unclear. To explore the molecular mechanisms in these events, in the present study we established a relevant in vivo model for selecting metastatic populations of ovarian cancer cells. Microarray and differential gene expression analysis of these cells indicate that autophagy is able to promote ovarian cancer malignancy. Therefore, animal experiments, cell-based characterization and gene correlation with patient survival were carried out at a later stage of this research.

2 | MATERIALS AND METHODS

2.1 | Cell lines and reagents

A2780 and SKOV-3 cells were originally obtained from ATCC. NIH:OVCAR-3 was purchased from the Bioresource Collection and Research Center, Taiwan. DMEM medium, RPMI 1640 medium, penicillin and streptomycin were purchased from Invitrogen. Rabbit anti–microtubule associated protein 1 light chain 3 (LC3) antibody, rabbit anti–p62 (SQSTM1) antibody and rabbit anti–ATG5 antibody were purchased from GeneTex. 3-methyladenine was purchased from Cayman Chemical. Other chemicals and reagents unless noted otherwise were purchased from Sigma. The lentivirus containing sh*ATG5* (clone TRCN0000151474) was kindly provided by Dr Sheng-Hui Lan from National Yang-Ming University.

2.2 | Animal ethics and treatments

BALB/c nude female mice (6-8 weeks old) were purchased from BioLASCO. All the in vivo experiments were approved by the Institutional Animal Care and Use Committee of the National Yang-Ming University (approval number: 1011231).

To establish the in vivo selection model, ovarian cancer cells were harvested, washed and adjusted to appropriate numbers in PBS. For selection of metastases, A2780 (1 x 10^7 cells), SKOV-3 (1 x 10^7 cells) or NIH:OVCAR-3 (1 x 10^7 cells) were injected intraperitoneally into female nude mice (n = 3). To increase the metastatic ability of NIH:OVCAR-3, another strategy that used cancer spheroids was also tested. Briefly, NIH:OVCAR-3 cells (4 x 10^6 cells) were cultured in polyhydroxyethylmethacrylate-coated Petri dishes for 3 days to allow formation of multicellular spheroids.[15] The collected spheroids, containing 1 x 10^7 cells, were used for intraperitoneal injection. To obtain tumor-derived cancer cells, mice were killed at specific times after xenograft: 21 days for A2780, 35 days for SKOV-3 and 49 days for NIH:OVCAR-3. Peritoneal metastatic nodules were collected, minced and cultured. After 24 hours, the medium was refreshed to remove non-adhered tissue debris and cells. Each subsequent intraperitoneal metastatic cell generation is designated M1, M2 and M3.

To further compare the peritoneal implantation ability between different generations of cancer cells, A2780 (1 x 10^6 cells), SKOV-3 (4 x 10^6 cells), or their derived M3 generation was used for injection. To compare the subcutaneous growth ability of these cells, A2780 (5 x 10^5 cells), SKOV-3 (2 x 10^6 cells), or their derived M3 generation was used for injection. The tumor volume was calculated using the formula 0.52 × length x width^2 at indicated intervals. At the endpoints, the final volume of isolated tumors was measured.

2.3 | RNA preparation, gene quantification and microarray

Total RNA from cancer cell lines were extracted by TRIzol (Invitrogen) according to the manufacturer's instructions. For gene quantification, cDNA were synthesized using High-Capacity cDNA Reverse Transcription Kits (Life Technology) with oligo-dT primer. Gene quantification was performed using Power SYBR Green PCR Master Mix (Life Technologies) and calculated using the $2^{(-\Delta Ct)}$ formula. The primer pairs used for gene quantification are shown in Table S1. For microarray, total RNA were extracted from A2780 or A2780-M3. Microarray was performed by the National Yang-Ming University

VYM Genome Research Center using Affymetrix GeneChip Human U133 Plus 2.0 Array. Results were analyzed by Ingenuity Pathway Analysis.

2.4 | Bioinformatic analyses

Gene set enrichment analysis (GSEA) analysis was performed using version 3.0 of GSEA run on all the gene sets in version 6.0 of the Molecular Signatures Database (MSigDB).[16] To identify the differences between A2780 and A2780-M3, all 8 major gene set collections, including hallmark (H), positional (C1), curated (C2), motif (C3), computational (C4), gene ontology (GO; C5), oncogenic (C6) and immunogenic gene sets (C7), were applied (http://software.broadinstitute.org/gsea/msigdb/index.jsp). $P < .05$ is set as the cutoff for the significance level and a false discovery rate (FDR, q-value) with ≤0.25 criterion is considered. Gene sets that passed the above thresholds were retained.

To analyze the correlation between expression of selected genes and survival data of ovarian cancer patients, Kaplan-Meier Plotter (http://kmplot.com/analysis/)[17] was applied. Briefly, the best specific probes (JetSet probes) for each gene were individually entered to obtain Kaplan-Meier plots. Information on overall patient survival was extracted. Log-rank analysis was used to determine statistical significance of the Kaplan–Meier survival curve ($P < 0.05$). Furthermore, information on hazard ratios (HR) with 95% confidence intervals was extracted.

2.5 | Proliferation and anchorage-independent growth assays

For the proliferation assay, A2780, SKOV-3 or their sublines at indicated density were seeded in 48-well plates. For low-density condition, cells were detached and collected at specific intervals. Cell numbers were counted under microscope. For high-density condition, cells were further incubated with 10% medium volume of AlamarBlue (AbD Serotec) at 37°C followed by detection of fluorescence intensities.

For the anchorage-independent growth, cells were resuspended with growth medium and seeded in 24-well dishes (2×10^3 per well) that were pre-coated with 30 mg/mL polyhydroxyethylmethacrylate. At specific intervals, cells were further incubated with 10% medium volume of AlamarBlue at 37°C followed by detection of fluorescence intensities.

2.6 | Immunofluorescent staining, puncta quantification and western blotting

For immunofluorescent staining, cells were cultured overnight on the coverslips precoated with 10% FBS. Cells were either serum-starved or treated with 20 μmol/L cisplatin for indicated intervals. After fixation with 4% paraformaldehyde for 30 minutes at room temperature, cells were then incubated under permeable (0.5% Triton X-100 in PBS) conditions for 5 minutes before further probing with primary antibodies against LC3 (1:100; GeneTex) or p62 (1:100; GeneTex) for 2 hours at room temperature followed by Alexa Fluor-conjugated secondary antibodies (1:200; Life Technologies). Nuclei were counterstained with DAPI. The images were acquired using a Zeiss LSM 700 confocal microscope. For quantification of LC3-II puncta formation, the number of punctate structures can be counted by using MetaMorph version 7.7 as the image analysis program.

For western blotting, cells collected at indicated intervals were lysed directly by sample buffer and sonicated for 5 seconds to fragmentate the genomic DNA. The above protein samples were boiled at 100°C for 5 minutes and analyzed by running 10% SDS-PAGE. Western blotting was performed using specific antibody against LC3, p62, ATG5 or β-actin.

2.7 | Statistical analysis

In the assays of gene quantification, cell proliferation and anchorage-independent growth, each treatment condition was performed in triplicate in an experiment. Data are presented as means ± SD. At least 3 independent experiments were repeated and these showed similar results. Data from in vivo mice experiments are shown as means ± SD. The mouse number used in each group was indicated. For other assays, such as western blot assessment and puncta quantification, at least 3 independent experiments were conducted for data collection and the statistical results are shown as means ± SE. For comparison between 2 groups, the unpaired Student's t test was used. For comparison of multiple groups, one-way ANOVA followed by Bonferroni post–test was used. For representative images of western blotting, at least 3 independent experiments showed similar results. No statistical method was used to predetermine sample size. No particular method of randomization was used in the experiments.

3 | RESULTS

3.1 | Selected metastatic sublines show more aggressiveness in vivo

To select more malignant sublines of cancer cells, 3 human ovarian cancer cells were subjected to intraperitoneal selection in nude mice (Figure 1A). The selection cycle was repeated 3 times for A2780 and SKOV-3 cells, and this yielded sublines that were designated A2780-M3 and SKOV-3-M3, respectively. By way of contrast, NIH:OVCAR-3 showed low metastatic ability in nude mice; this resulted in a failure in the selection of sublines through the same protocol.

To determine whether the selected cells are more aggressive, A2780-M3, SKOV-3-M3 and their corresponding parental cells were injected intraperitoneally to compare their peritoneal implantation ability. In addition, these cells were xenografted subcutaneously to compare their tumorigenicity. Using the intraperitoneal metastasis model, there was no observable difference in the number of peritoneal metastases formed by A2780-M3 and A2780 (Figure 1B,C). However, when comparing the size of harvested tumor nodules, it revealed that the individual tumor volume of the A2780-M3 group

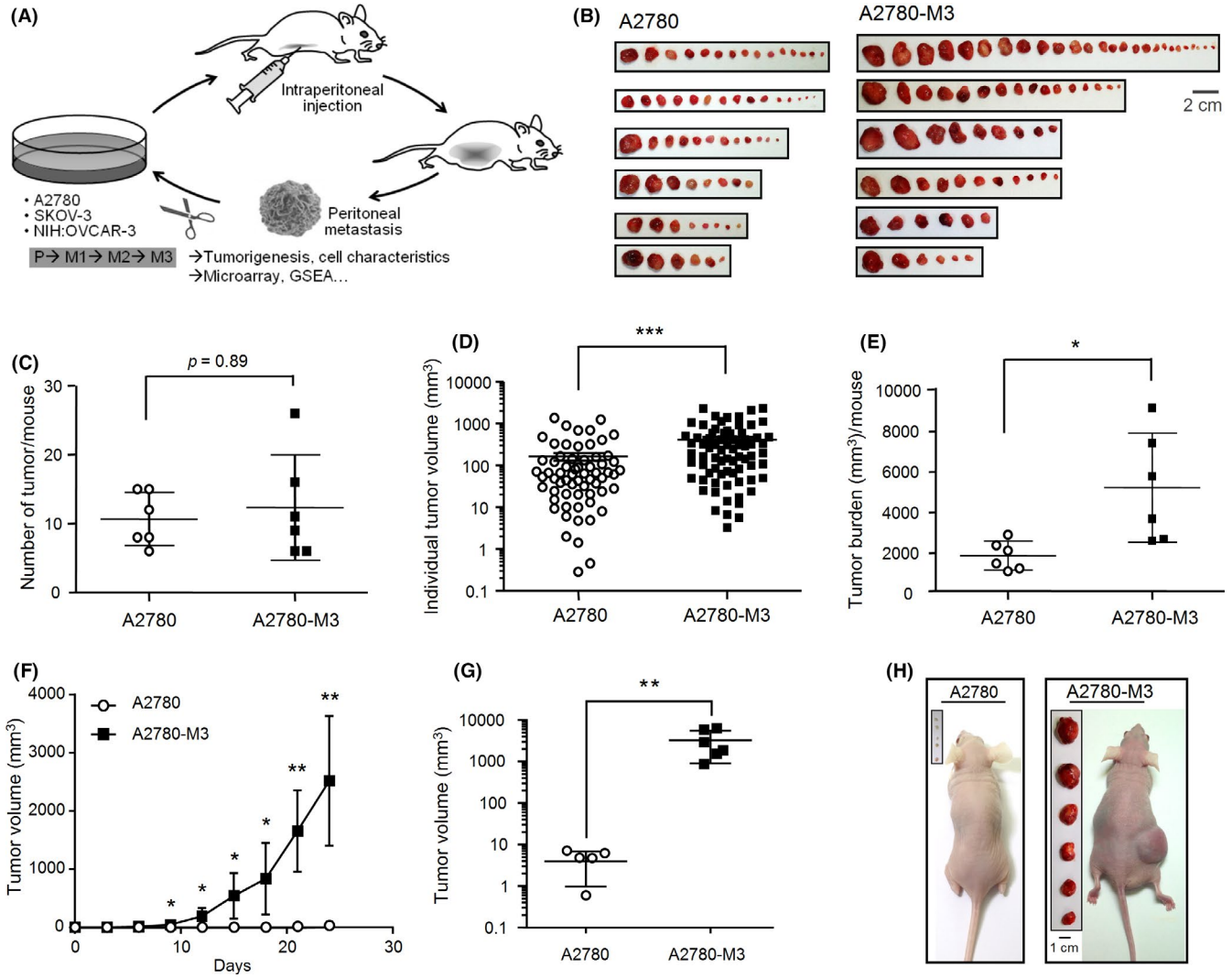

FIGURE 1 A2780-M3 derived by in vivo selection show enhanced tumorigenicity. A, The in vivo intraperitoneal selection scheme. Ovarian cancer cell lines were injected intraperitoneally into nude mice. The peritoneal metastases were isolated, minced and grown in culture medium to obtain new cell colonies. The selection procedure was repeated and the metastatic generations derived from parental cells (P) were sequentially designated M1, M2 and M3. The derived cells were either used for functional characterization or subjected to array and bioinformatic analyses. B-H, Comparison of the in vivo malignancy between A2780 and A2780-M3, the third metastatic generation. To compare the peritoneal implantation ability, nude mice injected with cancer cells intraperitoneally were killed at day 24 (n = 6). All peritoneal metastases were collected and photographed (B). Number of tumors per mouse (C), individual tumor volume (D) and total tumor burden per mouse (E) were compared. To compare the tumorigenic ability between these 2 cell lines, nude mice were xenografted subcutaneously. Changes in the tumor volume (F) were measured every 3 days and the final volumes of tumors harvested at the endpoint (G) were compared. For each group, the isolated tumors from mice (n = 5 for A2780 and n = 6 for A2780-M3) and a representative mouse at the endpoint were photographed (H). *P < .05, **P < .01, ***P < .001

was significantly higher than that of the A2780 control group (Figure 1D). The average tumor burden per mouse was also significantly increased for the A2780-M3 group (Figure 1E). Using the subcutaneous injection model, the tumors formed by A2780-M3 cells could be detected at day 9 after xenograft and the volumes of these tumors continued to increase in a time-dependent manner. By way of contrast, no apparent tumor nodules could be observed when the A2780 control group was examined (Figure 1F). A further analysis of the final volume of the tumors harvested from the killed mice indicated that there is a significant increase in the A2780-M3 group compared to its control (Figure 1G,H).

We also applied the same protocols to compare the changes in characteristics between SKOV-3-M3 and SKOV-3 in vivo. Using the intraperitoneal metastasis model, the SKOV-3-M3 group yielded more metastatic nodules when compared to the SKOV-3 control (18.0 ± 6.7 vs 10.5 ± 6.1; P < 0.05) (Figure S1A). In contrast to the above, there was no observable difference in the individual volume of the harvested tumors (Figure S1B) or in the total tumor burden per mouse (Figure S1C) between these 2 groups. Using the subcutaneous injection model, although the estimated tumor growth rate of the SKOV-3-M3 group was higher than that of the SKOV-3 control, no significant difference can be observed in the

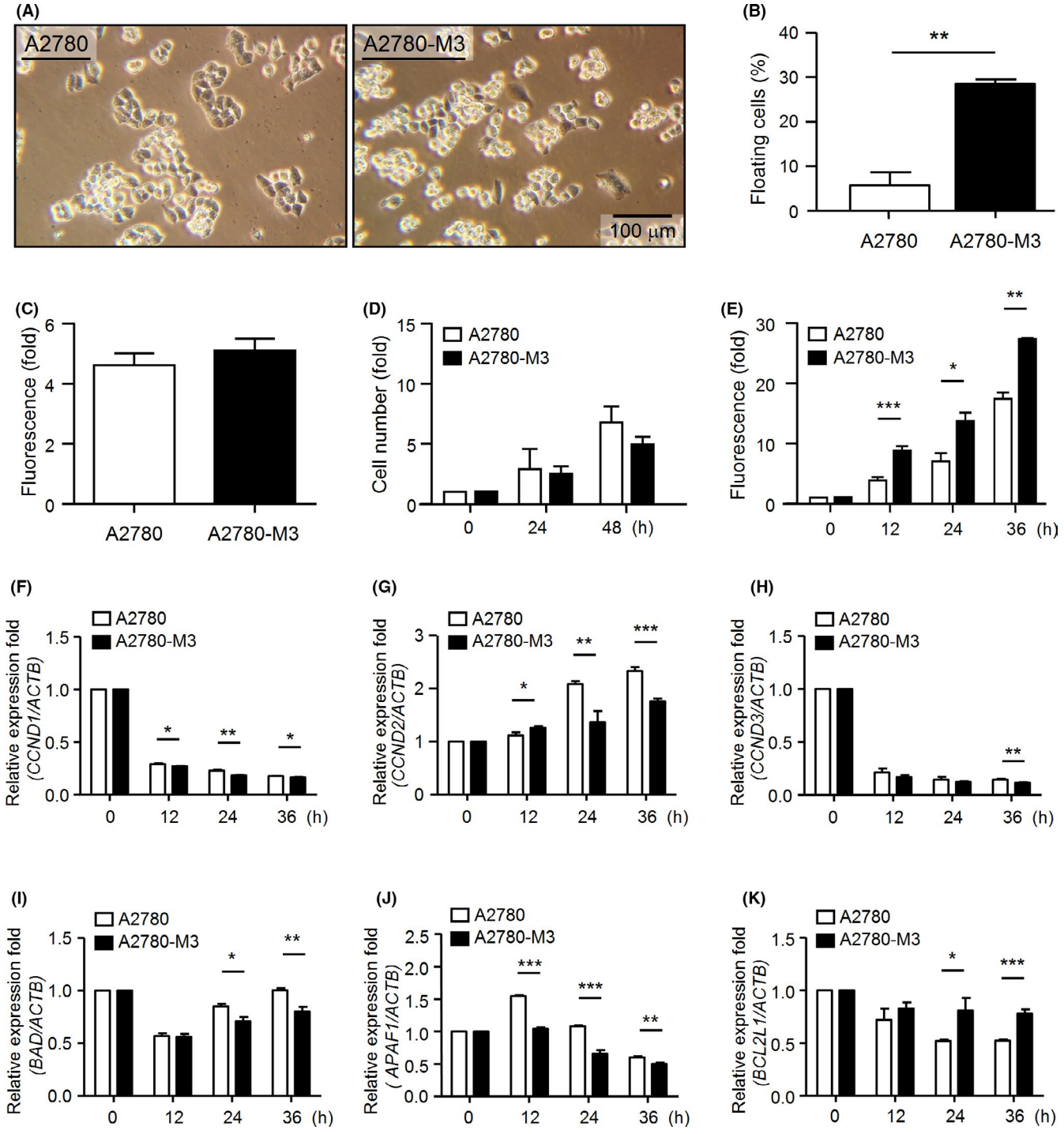

FIGURE 2 Characterization of the cell behaviors of parental and selected A2780 cells. A, Cells (5 x 10^4 cells/cm^2) plated on 2D culture dishes were cultured overnight and then photographed. B, The attached and floating cells in the above cultures were then separated to allow counting and the floating percentage was calculated. C, Anchorage-independent growth assay. Cells were cultured in polyhydroxyethylmethacrylate-coated plates for 2 days. The growth rates were compared using the AlamarBlue assay. The fluorescence value of the cells at day 0 served as the one-fold control. D, E, Growth potency under different cell densities. Cells seeded at normal density (5 x 10^4 cells/cm^2) (D) or at high density (5 x 10^6 cells/cm^2) (E) were further cultured for different time intervals. The growth rates were compared by cell counting or the AlamarBlue assay. The cell number or fluorescence value of the cells at day 0 served as the one-fold control values. F-K, Cells seeded at high-density condition (5 x 10^6 cells/cm^2) were further cultured for different intervals. The cell proliferation-related genes, including *CCND1* (F), *CCND2* (G) and *CCND3* (H), and the apoptosis-related genes, including *BAD* (I), *APAF1* (J) and *BCL2L1* (K), were quantified by real-time PCR. Data were normalized against the *ACTB* level. Data are means ± SD. **P* < 0.05, ***P* < 0.01, ****P* < 0.001

final volume of tumors harvested at day 54 after xenograft (Figure S1D and S1E). Taken together, these results indicated that selected ovarian cancer cells show greater aggressiveness in some aspects in vivo compared to their parental controls; however, the changes in malignant behaviors that occur seem to vary along with the cell line used for selection. Specifically, the selected A2780 subline showed an increase in tumor growth ability, whereas the selected SKOV-3 subline yielded more metastatic nodules during peritoneal dissemination.

3.2 | Selected ovarian cancer cells show changes in different behaviors in vitro

Based on the above results, it seems that the selected cancer cells would vary in certain cell characteristics in vitro. Indeed, initially we were able to observe a morphological change in the selected A2780 subline. Whereas parental A2780 cells grew while adhering to the tissue culture dishes, A2780-M3 cells tended to form clusters with a round cellular morphology (Figure 2A,B). In contrast, no apparent morphological difference could be observed between SKOV-3 and SKOV-3-M3 (Figure S2A).

Next, the cell growth abilities were compared using various assays. Using the anchorage-independent growth assay, whereas A2780 and A2780-M3 showed similar abilities (Figure 2C), SKOV-3-M3 exhibited a higher ability to undergo anchorage-independent growth compared to SKOV-3 (Figure S2B); this is able to partially explain why SKOV-3-M3 cells form more metastases in the intraperitoneal dissemination model in vivo (Figure S1A). However, it should be noted that, under the 2D-culture condition, the growth rate of A2780-M3 was similar to that of A2780 when the cells were plated at normal density (5 x 10^4 cells/cm^2) (Figure 2D). In contrast, A2780-M3 grew much faster than A2780 when they were plated at high density (5 x 10^6 cells/cm^2) (Figure 2E). Nonetheless, when SKOV-3 and SKOV-3-M3 were compared, they exhibited similar growth rates under either condition (Figure S2C and S2D).

We further investigated the potential mechanism by which A2780-M3 had acquired higher growth ability under the stress from a high cell density. When A2780-M3 was compared with parental A2780 in high-density cultures, A2780-M3 showed no apparent and consistent increase in the expression of various proliferation markers, such as *CCND1*, *CCND2* and *CCND3* (Figure 2F-H). By way of contrast, in A2780-M3, we were able to observe decreases in the expression of *BAD* and *APAF1*, which are the pro–apoptotic makers, as well as an increase in *BCL2L1*, an anti–apoptotic marker (Figure 2I-K). Taken together, our findings suggest that A2780-M3 displays an increased potential for anti–apoptosis, and that this might help to sustain their survival and growth when placed under high stress due to a high cell density.

3.3 | Autophagy-related genes are enriched in A2780-M3

The above findings suggest that A2780-M3 shows conspicuous increases in tumorigenicity in vivo (Figure 1) and in anti–apoptotic growth ability in vitro (Figure 2). Therefore, we were particularly interested in pinpointing the molecular changes that underlie these phenomena. To do this, cDNA microarray (Affymetrix GeneChip Human Genome U133 Plus 2.0 Array) technology was first applied to determine which genes are differentially expressed between A2780-M3 and its parental A2780. The dataset is available as Table S2. To investigate the potentially altered pathways, the resulting data were further processed by GSEA using gene sets from the MSigDB.[16] An overview of the top 20 gene sets enriched in A2780-M3 is presented in Table S3. We were looking for gene sets involved in cancer progression. In the GO category (MSigDB C5; included 1454 gene sets), we identified that the autophagosome-related genes were enriched in A2780-M3 compared to A2780 (normalized enriched score (NES) = 1.87; FDR = 0.13) (Figure 3 and Table S3). The information available on these genes and their rank metric scores are presented in the additional information (Table S4). These findings suggest that

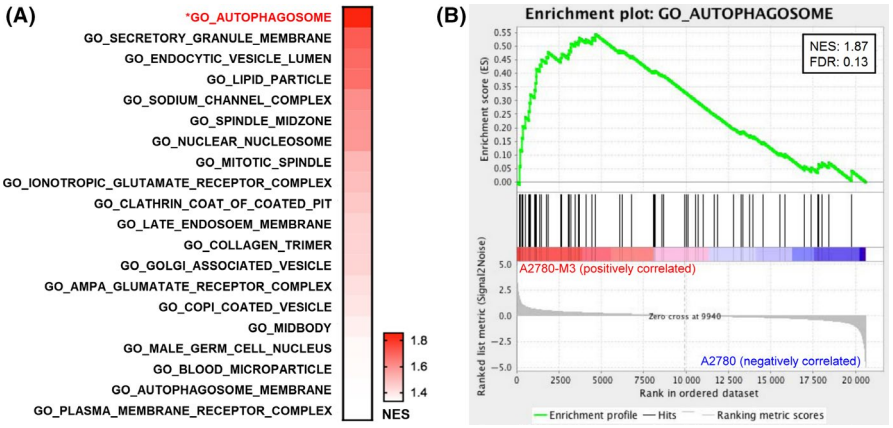

FIGURE 3 Identification of the gene sets enriched in A2780-M3. A, Gene set enrichment analysis (GSEA) was applied. The top 20 enriched gene sets in the category of gene ontology (GO) were ranked using their normalized enriched scores (NES) and shown on a heat map. The GO_AUTOPHAGOSOME set showed the highest NES for A2780-M3. B, The enrichment plot of GO_AUTOPHAGOSOME. The bottom portion showed the gene hits and their rank metric scores moving down the list of ranked genes

A2780-M3 has a higher autophagy potential and, thus, may tend to undergo autophagy when exposed to stresses.

3.4 | Selected metastatic cell variants tend to undergo autophagy under stress

To verify the above hypothesis, several different stress conditions were applied. Under normal conditions, compared to A2780, A2780-M3 was shown to have an equivalent amount of LC3-II but had a higher basal level of p62; however, after being cultured at high density (5 x 10^6 cells/cm^2) for 12 hours, more LC3-II and less remaining p62 were found to be present in A2780-M3 compared to A2780 (Figure 4A-D). Similarly, at normal density (5 x 10^4 cells/cm^2), A2780-M3 also showed a greater accumulation of LC3-II amount than parental A2780 when other stress conditions were applied, such as serum starvation (Figure 4E,F) and cisplatin treatment (Figure 4G,H).

For further confirmation, the formation of autophagic puncta in cells was measured. Indeed, A2780-M3 exhibited more autophagic puncta than A2780 when starved or when treated with cisplatin (Figure 4I,J). Incidentally, puncta observation was not able to be carried out at the high cell-density condition because of the presence of severe cell aggregation and image overlap. Taken together, these results suggest that selected A2780-M3 cells tend to undergo autophagic induction when they meet a variety of stress conditions.

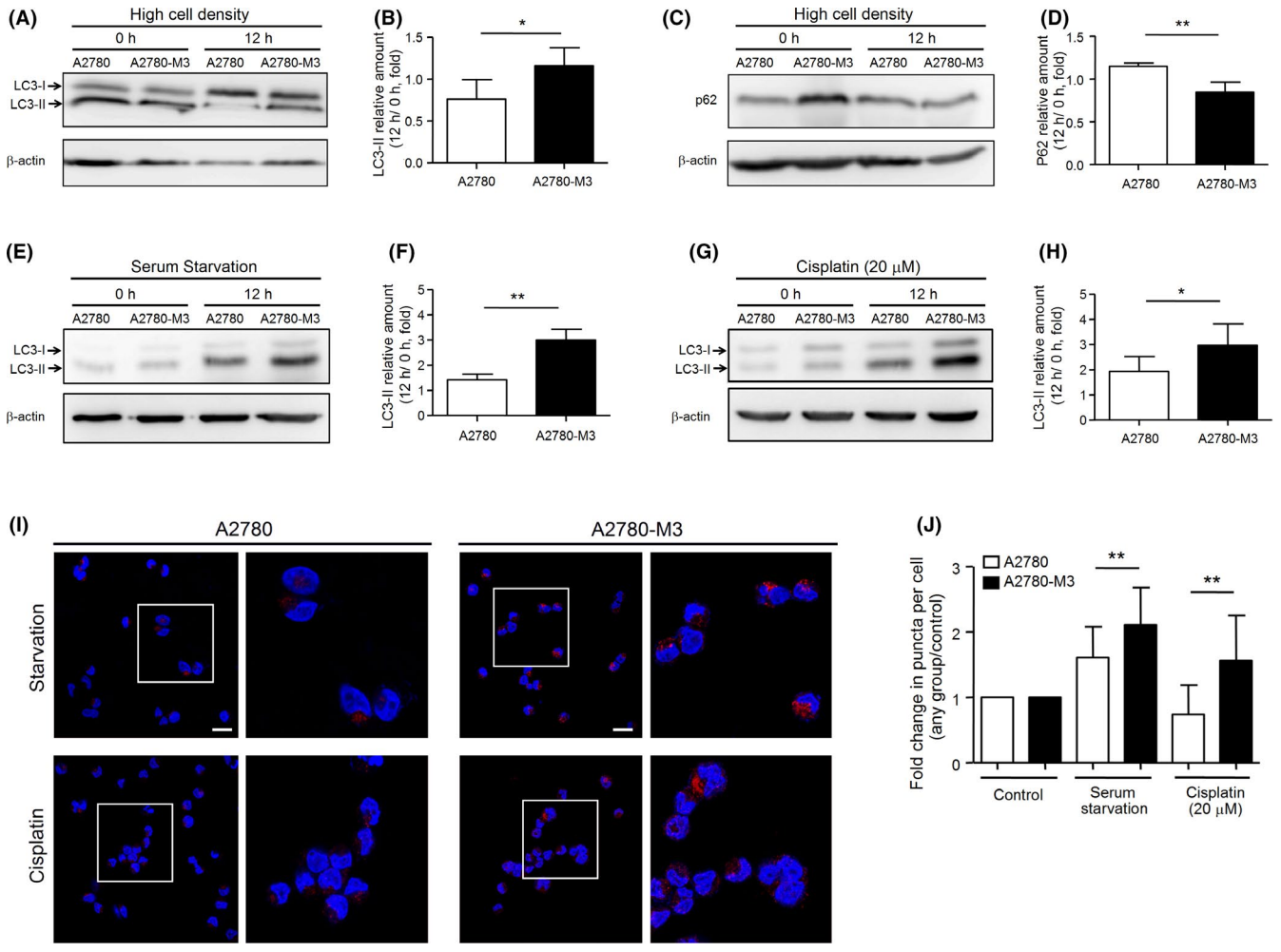

FIGURE 4 A2780-M3 exhibits a higher autophagic ability under different stresses. A-D, Cells seeded at high density (5 x 10^6 cells/cm^2) were harvested at indicated intervals. The amounts of LC3-II (A, representative image; B, quantification) and p62 (C, representative image; D, quantification) were compared between groups. E-H, Cells seeded at normal density were either starved (E, representative image; F, quantification) or treated with cisplatin (G, representative image; H, quantification) for indicated intervals. The amounts of LC3-II were compared. For western blotting, β-actin was used as a loading control for normalization. Quantification is shown as means ± SE of at least 3 independent experiments. I,Cells seeded at normal density were cultured in complete medium (control), medium without serum (starvation; upper panel) or medium with 20 μmol/L cisplatin (lower panel) for 12 h. The cells were then fixed and stained to detect LC3-II puncta (red). The merged images include DAPI staining (blue). One representative image is shown for each group. J, For quantification, the numbers of LC3-II puncta per cell were quantified using MetaMorph. Around 100 cells were analyzed in each group per experiment. Data were first normalized against their control groups (one-fold) and the results were then expressed as fold changes. Quantification is shown as means ± SE of 3 independent experiments. *$P < .05$, **$P < .01$

In addition to the above, changes in autophagic ability were also assessed for SKOV-3 and. SKOV-3-M3. As expected, SKOV-3-M3 cells accumulated more LC3-II protein fragments than SKOV-3 cells under either serum starvation (Figure S3A and S3B) or cisplatin treatment (Figure S3C and S3D). Consistently, as compared to parental SKOV-3, more autophagic puncta were formed in SKOV-3-M3 when these cells encountered the above stress conditions (Figure S4). To sum up, our findings lead us to the conclusion that the selected metastatic cell variants, namely A2780-M3 and SKOV-3-M3, show a tendency to undergo autophagic induction under stress conditions.

3.5 | Autophagy contributes to the growth effect of A2780-M3 cells when under the stress due to high density

Previously, A2780-M3 was characterized as having acquired higher growth ability when under stress due to a high cell density (Figure 2E). We further verified whether high autophagic potency contributes to this phenomenon. Using the cell growth assay, it was found that addition of an autophagic inhibitor, either 3-methyladenine (3-MA) (Figure 5A) or wortmannin (Figure 5B), indeed significantly dampened the growth of A2780-M3 but not that of parental A2780 cells. A similar effect could be seen when *ATG5* was knocked down in these cells (Figure 5C). In A2780-M3 cells cultured for 24 hours, knockdown of *ATG5* did not show a distinct change in the expression of apoptosis-related makers (Figure S5). Taken together, these findings suggest that autophagy contributes to the growth potency of A2780-M3 under the stress of high cell density.

3.6 | Enriched autophagy-related genes in A2780-M3 show prognostic significance regarding ovarian cancer progression

The above results lead us to the conclusion that an acquirement of autophagic ability by ovarian cancer cells will promote their aggressiveness in vivo. To make these results more clinically relevant, we further assessed the relationships between the autophagy-related genes enriched in A2780-M3 and the overall survival of ovarian cancer patients using Kaplan-Meier Plotter,[17] in which 1656 cases of ovarian cancer patients were included. Of interest, the expression levels of 73% (22 out of 30) of genes were significantly co–related with the patients' overall survival rate ($P < 0.05$) (Figure 6A-C). Detailed information of the various *P*-values and hazard ratios for each gene are provided in the additional information (Table S5). Taken together, the above findings provide clinical support that autophagy is involved in ovarian cancer progression in humans.

4 | DISCUSSION

Ovarian cancer is the most lethal gynecologic malignancy. Currently, genomic and bioinformatic approaches that analyze genetic profiling on single biopsy tissues or biopsy tissues from different cancer stages are often used as the standard approaches for the assessment of molecular pathways or biomarkers important to ovarian cancer progression. However, ovarian cancer is a very heterogeneous disease in which different histological types may result from different origins and, thus, have distinct genetic patterns.[18] Therefore, most conventional investigations lack appropriate origin controls for pathological comparison. For this reason, the in vivo selection model proposed in our study, which

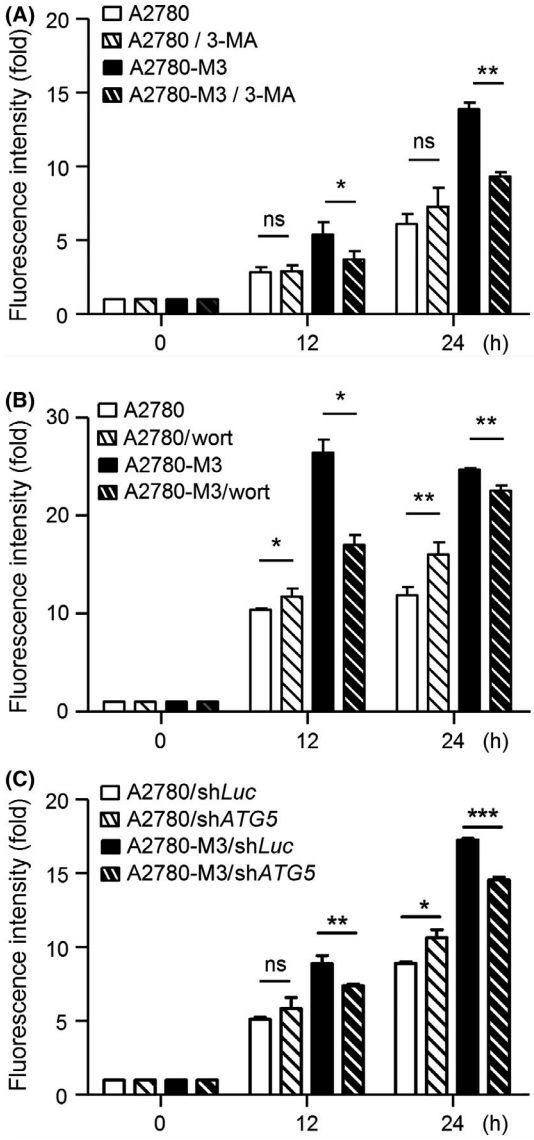

FIGURE 5 Inhibition of autophagy dampens the growth ability of A2780-M3 at high density. For inhibitor treatments, cells seeded at high density (5 x 106 cells/cm^2) were treated without or with 1 of 2 autophagic inhibitors, 3-MA (A) or wortmannin (wort) (B). C, For knockdown experiments, control cells with luciferase (*Luc*) knockdown or cells with *ATG5* knockdown were seeded at high density. Cell viability was assessed at indicated intervals using AlamarBlue reagent. The fluorescence value of the cells in each group at day 0 served as the one-fold control for data normalization. Data are shown as means ± SD. **P* < .05, ***P* < .01, ****P* < .001

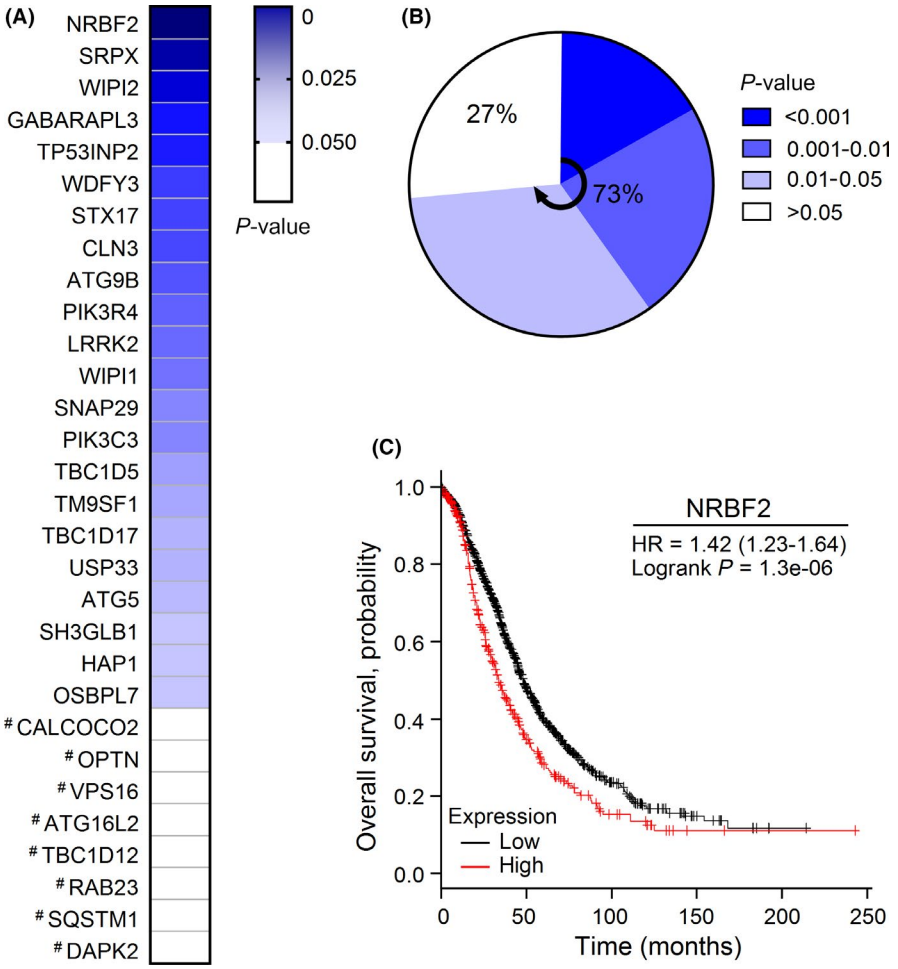

FIGURE 6 Correlation between enriched autophagy-related genes and the clinical prognosis of ovarian cancer patients. A, A list of autophagy-related genes enriched in A2780-M3. Correlations between gene expression and the probability of overall survival of ovarian cancer patients (n = 1656) were analyzed using Kaplan-Meier Plotter. Genes were sorted by their *P*-values in a heat-map manner. #, $P > 0.05$. B, Pie chart of the *P*-value distribution. The expression levels of 73% genes were significantly correlated to the overall survival of ovarian cancer patients ($P < 0.05$). C, Kaplan-Meier curve of *NRBF2*, which exhibited the lowest *P*-value in the above assay

aims to generate sequential malignant metastases from the same cell line origin, may be a solution to this problem. Analysis of these derived malignant sublines would greatly advance our understanding of the genetic and molecular determinants crucial to cancer progression. Previously, a study that applied an ovarian clear-cell carcinoma cell line RMG-1 to in vivo selection suggests that Le^x-determinant on the cell surface is involved in the adhesion of cancer cells during dissemination[19]; however, detailed mechanisms such as the transcriptional changes and the involved glycoproteins in selected cancer cells have not yet been explored. Using our in vivo peritoneal dissemination model, we identified that autophagy-related genes were enriched in A2780-M3 cells. A2780-M3 cells tended to undergo autophagic induction upon exposure to different stress conditions. Autophagy is now known as a double-edged sword involved in both cell survival and death.[20] At the high-density stress condition, we also, intriguingly, noticed that parental A2780 and A2780-M3 behaved differently (Figure 5; and Figure S5). A2780-M3 cells kept proliferate, whereas blockage of autophagy, by either autophagic inhibitors or *ATG5* knockdown, efficiently reversed this phenomenon. It also seems that the above treatments do not trigger apoptosis. Taken together, these data suggest that autophagy acts as a protector for A2780-M3 against the stress. By way of contrast, parental A2780 cells tended to grow better when blocking autophagy. It may be explained by the reason that parental A2780 cells would undergo autophagic cell death under the stress and, thereby, blockage of autophagy increases their growth ability. If this is true, then it raises another interesting question of how the abdominal microenvironment switches the autophagic death role towards survival in selected cancer cells.

In our results, we also found that selected SKOV-3-M3 is more sensitive to autophagic induction upon exposure to diverse stress conditions. However, cell-based and animal experiments indicate that selected SKOV-3-M3 acquired a higher ability to form more metastases but not to increase the tumor size, which is what occurred with A2780-M3. This might be because these 2 cell lines originate from different histological subtypes and, thus, inherit distinct metastasis-related characteristics.[21] Intriguingly, it also raises another question of whether increased autophagic response of SKOV-3-M3 cells contributes to the increase in the number of metastases in vivo. Although more studies are needed to solve this issue, previous reports have suggested that autophagy contributes to the dormancy and survival of SKOV-3 cells.[22,23] When SKOV-3 cells encounter some stress conditions, such as nutrient deprivation, autophagy induced by certain tumor suppressor machinery enables these cells to remain dormant[23]; this may allow SKOV-3 cells to evade anoikis

when they are xenografted into mice in vivo.[22] After succeeding in invasion, reduction in the suppressor machinery would allow the xenografts to grow rapidly. Thus, the above effect may partially explain our result that SKOV-3-M3 forms more metastases than SKOV-3 in the intraperitoneal xenograft model.

In addition to the above, accumulating findings have also demonstrated that autophagy acts as a protector for ovarian cancer cells to desensitize these first-line drugs, such as cisplatin and paclitaxel. For example, ERK pathway-induced autophagy may counteract cisplatin-induced cell death in OV433 cells,[24] whereas YAP-activated autophagy may contribute to cisplatin resistance in ovarian C13K cells.[25] In contrast, Zhang et al[26] showed that autophagy induced by thioredoxin domain containing 17 (TXNDC17) may promote paclitaxel resistance in SKOV-3 cells. The above diversities may derive from the ovarian cell types used in the experiments because different cell lines may inherit distinct genetic characteristics due to the high heterogeneity of ovarian cancer. Nevertheless, these studies clearly link coordination of autophagy with ovarian cancer progression and also support our results that A2780-M3 and SKOV-3-M3, although enhanced in different metastatic characteristics, both exhibit a higher autophagic response after *in vivo* selection.

In addition to autophagy, we found that several oncogenic signatures were also enriched in A2780-M3 cells when browsing the C6 oncogenic gene sets in the MSigDB collections (Table S6). Some of the gene sets, such as KRAS.DF.V1_UP, AKT_UP.V1_DN and YAP1_UP, may be predictable to be enriched in A2780-M3 cells because they have been found by other studies to be important in ovarian cancer. For example, activating mutations and genomic amplifications of *KRAS* have been found with a significantly higher frequency in ovarian cancer.[27,28] In high-grade serous ovarian cancer, amplification in *AKT* isoforms occurs in around 15% of cases.[27] Furthermore, a nuclear YAP signal can be detected in 98% of patients with ovarian serous cystadenocarcinoma.[29] The above genes have also been well known to play critical roles in the development and progression of many other cancers. More intriguingly, increasing evidence further indicates that the signals of these genes are involved in autophagy. Apparently, RAS activation upregulates basal autophagy in diverse cancer cells.[30] In the gene set of KRAS.DF.V1_UP, non-canonical IkappaB kinase TBK1 is selectively essential in cancer cells that contain mutant KRAS,[31] whereas TBK1 directly controls autophagosomal engulfment of selected substrates through phosphorylating p62.[32] In addition, AKT1 has been reported to play a key mediator in KRAS oncogene-induced autophagy in some cancer cells.[33] As to YAP, it has been proven that this gene promotes the survival of diverse cancer cells through activation of autophagic flux.[25,34] Therefore, it will be of great interest to characterize the molecular mechanisms that link the enriched oncogenic gene sets found in A2780-M3 cells to the induction of autophagy in the ovarian cancer; these findings should provide new insights into the relationship between autophagy and ovarian cancer malignancy.

DISCLOSURE

The authors have no conflict of interest to declare.

ORCID

Ching-Wei Luo https://orcid.org/0000-0003-3956-2935

REFERENCES

1. Torre LA, Bray F, Siegel RL, Ferlay J, Lortet-Tieulent J, Jemal A. Global cancer statistics, 2012. *CA Cancer J Clin*. 2015;65:87-108.
2. Feeley KM, Wells M. Precursor lesions of ovarian epithelial malignancy. *Histopathology*. 2001;38:87-95.
3. Siegel RL, Miller KD, Jemal A. Cancer statistics, 2018. *CA Cancer J Clin*. 2018; 68: 7-30.
4. Cannistra SA. Cancer of the ovary. *N Engl J Med*. 2004;351:2519-2529.
5. Lengyel E. Ovarian cancer development and metastasis. *Am J Pathol*. 2010;177:1053-1064.
6. Gupta GP, Massague J. Cancer metastasis: building a framework. *Cell*. 2006;127:679-695.
7. Ayantunde AA, Parsons SL. Pattern and prognostic factors in patients with malignant ascites: a retrospective study. *Ann Oncol*. 2007;18:945-949.
8. Kipps E, Tan DS, Kaye SB. Meeting the challenge of ascites in ovarian cancer: new avenues for therapy and research. *Nat Rev Cancer*. 2013;13:273-282.
9. Cai Q, Yan L, Xu Y. Anoikis resistance is a critical feature of highly aggressive ovarian cancer cells. *Oncogene*. 2015;34:3315-3324.
10. Ahmed N, Thompson EW, Quinn MA. Epithelial-mesenchymal interconversions in normal ovarian surface epithelium and ovarian carcinomas: an exception to the norm. *J Cell Physiol*. 2007;213:581-588.
11. Ahmed N, Stenvers KL. Getting to know ovarian cancer ascites: opportunities for targeted therapy-based translational research. *Front Oncol*. 2013;3:256.
12. Fidler IJ, Kripke ML. Metastasis results from preexisting variant cells within a malignant tumor. *Science*. 1977;197:893-895.
13. Heppner GH. Tumor heterogeneity. *Cancer Res*. 1984;44:2259-2265.
14. Fidler IJ, Hart IR. Biological diversity in metastatic neoplasms: origins and implications. *Science*. 1982;217:998-1003.
15. Davidowitz RA, Iwanicki MP, Brugge JS. In vitro mesothelial clearance assay that models the early steps of ovarian cancer metastasis. *J Vis Exp*. 2012;60:e3888. https://doi.org/10.3791/3888
16. Subramanian A, Tamayo P, Mootha VK, et al. Gene set enrichment analysis: a knowledge-based approach for interpreting genome-wide expression profiles. *Proc Natl Acad Sci U S A*. 2005;102:15545-15550.
17. Lanczky A, Nagy A, Bottai G, et al. miRpower: a web-tool to validate survival-associated miRNAs utilizing expression data from 2178 breast cancer patients. *Breast Cancer Res Treat*. 2016;160:439-446.
18. Wang V, Li C, Lin M, et al. Ovarian cancer is a heterogeneous disease. *Cancer Genet Cytogenet*. 2005;161:170-173.
19. Kiguchi K, Iwamori M, Mochizuki Y, et al. Selection of human ovarian carcinoma cells with high dissemination potential by repeated passage of the cells in vivo into nude mice, and involvement of Le(x)-determinant in the dissemination potential. *Jpn J Cancer Res*. 1998;89:923-932.
20. Baehrecke EH. Autophagy: dual roles in life and death? *Nat Rev Mol Cell Biol*. 2005;6:505-510.
21. Hernandez L, Kim MK, Lyle LT, et al. Characterization of ovarian cancer cell lines as in vivo models for preclinical studies. *Gynecol Oncol*. 2016;142:332-340.

22. Lu Z, Luo RZ, Lu Y, et al. The tumor suppressor gene ARHI regulates autophagy and tumor dormancy in human ovarian cancer cells. *J Clin Invest*. 2008;118:3917-3929.
23. Lu Z, Baquero MT, Yang H, et al. DIRAS3 regulates the autophagosome initiation complex in dormant ovarian cancer cells. *Autophagy*. 2014;10:1071-1092.
24. Wang J, Wu GS. Role of autophagy in cisplatin resistance in ovarian cancer cells. *J Biol Chem*. 2014;289:17163-17173.
25. Xiao L, Shi XY, Zhang Y, et al. YAP induces cisplatin resistance through activation of autophagy in human ovarian carcinoma cells. *Onco Targets Ther*. 2016;9:1105-1114.
26. Zhang SF, Wang XY, Fu ZQ, et al. TXNDC17 promotes paclitaxel resistance via inducing autophagy in ovarian cancer. *Autophagy*. 2015;11:225-238.
27. Cheaib B, Auguste A, Leary A. The PI3K/Akt/mTOR pathway in ovarian cancer: therapeutic opportunities and challenges. *Chin J Cancer*. 2015;34:4-16.
28. Ross JS, Ali SM, Wang K, et al. Comprehensive genomic profiling of epithelial ovarian cancer by next generation sequencing-based diagnostic assay reveals new routes to targeted therapies. *Gynecol Oncol*. 2013;130:554-559.
29. Steinhardt AA, Gayyed MF, Klein AP, et al. Expression of Yes-associated protein in common solid tumors. *Hum Pathol*. 2008;39:1582-1589.
30. Schmukler E, Kloog Y, Pinkas-Kramarski R. Ras and autophagy in cancer development and therapy. *Oncotarget*. 2014;5:577-586.
31. Barbie DA, Tamayo P, Boehm JS, et al. Systematic RNA interference reveals that oncogenic KRAS-driven cancers require TBK1. *Nature*. 2009;462:108-112.
32. Matsumoto G, Shimogori T, Hattori N, Nukina N. TBK1 controls autophagosomal engulfment of polyubiquitinated mitochondria through p62/SQSTM1 phosphorylation. *Hum Mol Genet*. 2015;24:4429-4442.
33. Lo Re AE, Fernandez-Barrena MG, Almada LL, et al. Novel AKT1-GLI3-VMP1 pathway mediates KRAS oncogene-induced autophagy in cancer cells. *J Biol Chem*. 2012;287:25325-25334.
34. Song Q, Mao B, Cheng J, et al. YAP enhances autophagic flux to promote breast cancer cell survival in response to nutrient deprivation. *PLoS One*. 2015;10:e0120790.

SUPPORTING INFORMATION

Additional supporting information may be found online in the Supporting Information section at the end of the article.

How to cite this article: Kuo C-L, Jiang Z-Y, Wang Y-W, et al. In vivo selection reveals autophagy promotes adaptation of metastatic ovarian cancer cells to abdominal microenvironment. *Cancer Sci*. 2019;110:3204–3214. https://doi.org/10.1111/cas.14162